Competing Electronic Ground States in the Heavy-Fermion Superconductor $CeRh_2As_2$

Joanna Bławat,[1,*] Grzegorz Chajewski,[2] Daniel Gnida,[2] John Singleton,[1] Oscar Ayala Valenzuela,[1] Dariusz Kaczorowski,[2] and Ross D. McDonald[1,†]

[1]*National High Magnetic Field Laboratory, Los Alamos National Laboratory, Los Alamos, New Mexico 87545, USA*

[2]*Institute of Low Temperature and Structure Research, Polish Academy of Sciences, ul. Okólna 2, 50-422 Wrocław, Poland*

(Received 30 January 2025; revised 31 October 2025; accepted 21 November 2025; published 29 December 2025)

$CeRh_2As_2$ is rare among superconductors, in that the magnetic field tunes it between two distinct superconducting phases. Combined with a lack of local inversion symmetry and an upper critical field exceeding the Pauli paramagnetic limit, this excitingly suggests triplet multicomponent superconductivity. Preceding the superconducting onset, f-electron correlations cause long-range order, attributed both to local antiferromagnetism and itinerant (quadrupole) density waves. A magnetic field provides a significant perturbation of the f electrons and may reveal the nature of the many-body correlations. Therefore, we report comprehensive magnetization and magnetotransport studies on microstructured devices in fields of up to 73 T. Applied along the c axis, the field causes a low-temperature change of majority (hole) carrier density at $\mu_0 H \approx 24$ T. By contrast, in-plane fields produce a cascade of phase transitions; the field-induced in-plane conductivity anisotropy and lack of accompanying magnetic features, plus the closed-dome nature of the overall phase boundary is consistent with a hierarchy of field-induced density-wave states.

DOI: 10.1103/m44c-tzrj

Subject Areas: Condensed Matter Physics, Strongly Correlated Materials, Superconductivity

I. INTRODUCTION

The electronic ground states in Ce-based heavy-fermion compounds are highly sensitive to the strength of coupling between f-electron orbitals and other bands, resulting in the formation of states ranging from long-range magnetic order to unconventional superconductivity or non-Fermi liquid behavior [1]. Furthermore, the energy differences between these states are frequently small, so that the compound's behavior is easily tuned by changes in composition, applied pressure, and/or magnetic field [1–3]. As a result, such materials offer the possibility to study the interplay between competing orders in a single strongly correlated system. In addition to chemical doping and external pressure, high magnetic fields can induce valence transitions in Ce compounds. For example, fields induce either f-electron localization (e.g., elemental Ce, $CeOs_4Sb_{12}$) or delocalization ($CeCoIn_5$ [2]). Moreover, akin to the application of pressure, the field can induce quantum critical behavior [4,5], nematicity [6,7], density waves [8], and unconventional superconductivity [3,9], all of which challenge current understanding.

Previous observations of multiphase superconductivity in heavy-fermion systems are generally restricted to Uranium compounds (e.g., UTe_2, UPt_3 [9–12]). However, recently $CeRh_2As_2$ was shown to exhibit multiple superconducting phases below $T_c = 0.26$ K [10]; a magnetic field applied along the c axis is thought to induce a transition from an even-parity to an odd-parity superconducting state at around 4 T [10]. The higher-field phase has an upper critical field of 14 T, exceeding the Pauli limit [10]. In addition, $CeRh_2As_2$ crystallizes in the centrosymmetric tetragonal $P4/nmm$ space group, with Ce occupying two positions with opposite Rh and As environments, breaking local inversion symmetry. These properties led to predictions of multicomponent triplet superconductivity with a complex order parameter [13–17]. This fundamental materials research piqued the interest of the quantum-technology community; the bound states of topological superconductors are Majorana zero modes, leading to speculation that they are candidates for braiding quantum-computation schemes [14,18–21].

Preceding the onset of superconductivity, $CeRh_2As_2$ exhibits a second-order phase transition at $T_0 = 0.5$ K [22,23]. Initially, this was attributed to a quadrupole density wave

*Contact author: jblawat@lanl.gov

†Contact author: rmcd@lanl.gov

Published by the American Physical Society under the terms of the Creative Commons Attribution 4.0 International license. Further distribution of this work must maintain attribution to the author(s) and the published article's title, journal citation, and DOI.

(QDW) [10,24] of purely electronic origin; however, recent muon spin spectroscopy (μSR), nuclear magnetic resonance (NQR/NMR) and heat-capacity studies revealed that this transition also has an antiferromagnetic character. This may imply the coexistence below T_c of magnetic order, QDW, and superconductivity [22,25–27].

When the field is applied along the *a* axis, only the low-field superconducting phase is observed, with an upper critical field of 2 T [10,17]. This strongly anisotropic response is reflected in the field dependence of the magnetic ordered phase which is suppressed by the field applied along *c*, while it is stabilized to higher temperature by fields of up to 18 T [23,24] along the *a* axis. Although subject to extensive low-temperature and low-field experimental and theoretical studies, the origin of and relationship between the multiple phases exhibited by $CeRh_2As_2$ remain elusive.

Motivated by these phenomena, we report high magnetic field studies on $CeRh_2As_2$ that follow the trajectories of transitions observed below 18 T and investigate the relationship between various competing and coexisting phases using a magnetic field as a tuning parameter. We find a field-induced change of carrier density with $\mathbf{H}\|c$, while the in-plane configuration exhibits a cascade of field induced phases. By constructing the first high-field *T*-*H* phase diagrams of $CeRh_2As_2$, we reveal the subtle competition between correlated ground states and the role of magnetic field, not only in tuning the electron-electron pairing responsible for different symmetry superconducting states, but also favoring electron-hole pairing resulting in density waves. Field induced changes in *f*-electron localization driven by Kondo hybridization or a valence transition, and density waves induced by a magnetic field have been observed in $CeTIn_5$ (T = Ir, Rh, Co) suggesting that they might be a common feature among the heavy fermion unconventional superconductors.

II. FIELD INDUCED CHANGE OF CARRIER DENSITY

To help measure the magnetoresistivity tensor with current applied along specific crystallographic directions, and to increase the resistivity signal-to-noise ratio, focused ion beam (FIB) lithography was employed to fabricate devices with lateral dimensions ∼10 μm, resulting in 4-point resistances ranging from 100 mΩ to several ohms [28] with electric current flowing within the tetragonal *a*-*b* plane ($I\perp c$). To measure the resistance of $CeRh_2As_2$ with $\mathbf{H}\|c$, an 8 μm thick rectangular Hall bar 340 × 40 μm was used [see Fig. 1(a), inset]. The temperature dependent resistivity down to 50 mK is presented in Fig. 1(a). It exhibits typical heavy-fermion behavior; i.e., first $R(T)$ shows a shallow minimum on decreasing the temperature from 300 K, then forms a maximum at about 40 K, characteristic of the Kondo effect [1]. At low temperatures, there is a plateau below T_0 (marked with an arrow), and a sharp drop to zero resistance at $T_c = 0.3$ K related to

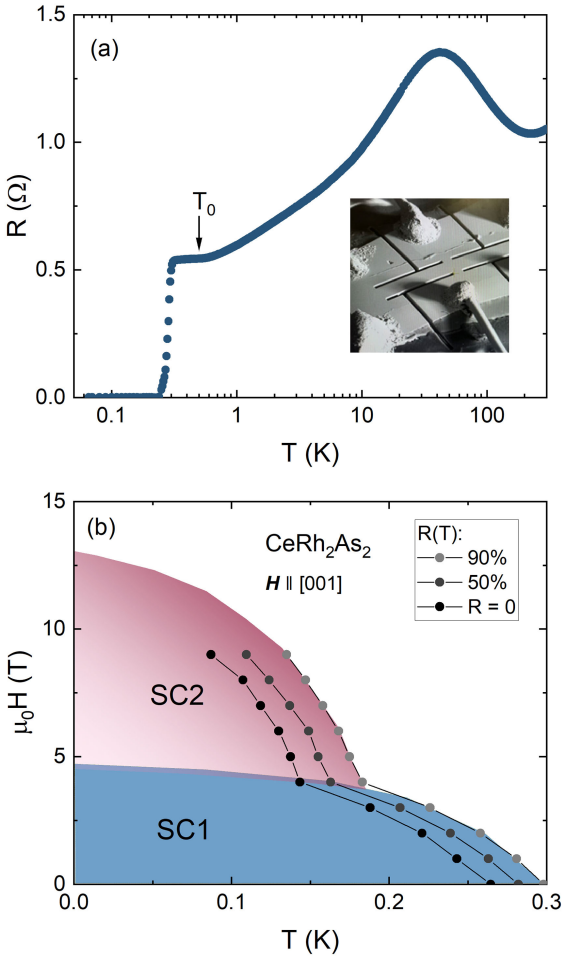


FIG. 1. (a) Resistance as a function of temperature measured on the FIB fabricated device. Inset: Electron micrograph of the focused ion beam defined Hall bar structure used for this measurement. (b) Low temperature phase diagram with $\mathbf{H}\|[001]$ created based on resistivity measurements on the FIB device showing two-phase superconductivity.

the superconducting transitions. The critical temperature is in a good agreement with those previously reported [10,22,25]. The residual resistivity ratio RRR = $R(300\text{ K})/R(0.5\text{ K}) = 2$, while in bulk $CeRh_2As_2$ single crystals the RRR was from 1.3 to 2.8 [25,29–32]. Investigations under fields of up to 14 T revealed the previously reported superconducting phases presented in Fig. 1(b). Our resulting phase diagram seems identical to that constructed earlier using transport, heat capacity, magnetization, and magnetostriction data from bulk crystals [10,17,23,24,30]. Therefore, our measurements suggest that the FIB process does not unduly alter the intrinsic properties of $CeRh_2As_2$.

Figure 2(a) shows magnetoresistivity [MR = $[R(H) - R(0)]/R(0)$, where $R(0)$ is the zero-field resistance] measured up to 60 T with $\mathbf{H}\|[001]$ at temperatures between 0.6 and 80 K. Below 1 K, negative magnetoresistance is observed at low fields, followed by a rise to a maximum

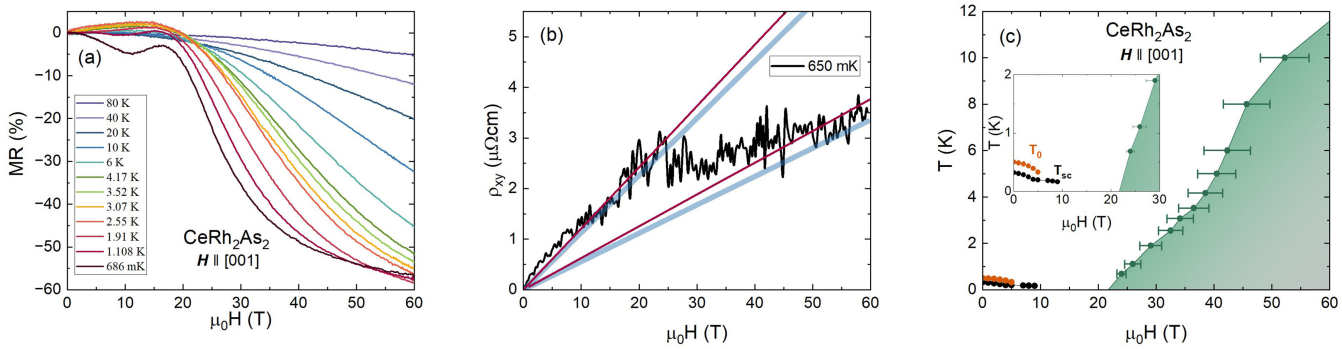


FIG. 2. (a) Magnetoresistance of $CeRh_2As_2$ measured up to 60 T for a range of temperatures between 600 mK and 80 K. (b) Hall effect (ρ_{xy}) as a function of magnetic field. Two-carrier analysis of the Hall data is given in the Supplemental Material, S4 [33], finding a dramatic increase in majority hole carrier density around 25 T. At both low and high field limits, the very small minority carrier densities (compared to those of the majority carriers) mean that single-carrier Hall fits provide a reasonable approximation (see S4 [33]) to the data. Consequently, the red lines represent straight-line fits through the origin to the low- and high-field ρ_{xy} data and the blue lines show single-carrier Hall predictions for exactly one (low field) and two (high field) holes per unit cell. (c) Magnetic field: temperature points bounding the region where the change of carrier density occurs are determined from the minimum in the first derivative of the magnetoresistance as described in the main text. The error bars represent the width of the transition, which is determined as 10% of the half-width of a Gaussian fit to the derivative of the magnetoresistance Fig. S2.

around 15 T. By contrast, for $1.2 < T < 4$ K the MR is small and positive up to $\mu_0 H \approx 20$ T, beyond which it drops drastically, reaching -60% at 60 T. Although the high-field MR becomes smaller with increasing temperature, it stays negative up to 80 K.

Figure 2(b) presents the low temperature Hall resistivity ρ_{xy} versus field. Throughout the measured temperature range ρ_{xy} remains positive, indicating that the dominant charge carriers are holes (see Fig. S2 [33]). However, at 0.65 K there is a marked change in the behavior of ρ_{xy} over a broad region of the field, centered on $\mu_0 H \approx 24$ T; the slope above $\mu_0 H \approx 40$ T is significantly smaller than that below 20 T. $CeRh_2As_2$ is almost certainly a multiband system, and so two different two-band Hall methods are justified and used in Supplemental Material [33] to fit the data. Both techniques strongly suggest that the majority carriers at both low and high fields are low-mobility holes; their density increases from approximately 5.5×10^{27} m^{-3} below 24 T (corresponding to about one hole per unit cell) to roughly 9×10^{27} m^{-3} (an average of the values from the methods in [33], and almost two holes per unit cell) well above 25 T. The majority-carrier holes are accompanied by very much smaller populations of higher mobility carriers; holes at low fields and electrons at high fields. A comparison of the Sommerfeld coefficient from heat capacity measurements with the low-field majority hole density and mobility (see Supplemental Material [33]) suggests an effective mass $m^* \approx 250 m_e$ (where m_e is the free-electron rest mass) and a scattering time $\tau \approx 5.5$ ps. These estimated values for m^* and τ are very comparable to those observed in other heavy-fermion systems [34]; the interactions that enhance the quasiparticle effective mass also suppress the scattering rate compared to those measured in more conventional metals.

In both low and high-field limits, the very small minority carrier densities (compared to those of the majority holes) mean that single-carrier Hall fits provide a reasonable approximation (see Supplemental Material, S4 [33]) to the data. These are shown in Fig. 2(b), where the red lines represent straight-line fits through the origin to the low and high-field ρ_{xy} data and the blue lines show single-carrier Hall predictions for exactly one (low field) and two (high field) holes per unit cell.

Because metals with relatively high carrier concentrations exhibit a tiny Hall signal, ρ_{xx} has a significantly better signal-to-noise ratio (Fig. S2 [33]). Consequently, to examine how the transition to increased hole density evolves with temperature and applied field we calculated the derivative dR_{xx}/dH_z from the resistance $R(H)$ measured at various temperatures (Fig. S2 [33]). The derivatives exhibit two main features: (i) a maximum at $\mu_0 H \approx 15$ T, which is observed only at 0.68 and 1.11 K; and (ii) a broad minimum at $\mu_0 H \approx 24$ T and 0.68 K (i.e., at the same field as the change in ρ_{xy} behavior) which moves towards higher fields with increasing temperature. Following the minimum in dR/dH to higher T results in the (H, T) phase boundary for $\mathbf{H} \| [001]$ shown in Fig. 2(c).

Taken together, the significant drop in the resistance and the low- and high-field slopes of ρ_{xy} correspond to an increased majority carrier (hole) concentration at high field. This change of carrier concentration suggests that the boundary in Fig. 2(c) corresponds to a transition at which f electrons are removed from the itinerant carrier population. Even considering the relatively small g factor of the cerium $4f$ states ($g = 1.1$ for $\boldsymbol{H} \| c$) [10] it is perhaps not surprising that the application of such strong magnetic fields has a profound effect upon their contribution to the Fermi surface. Interestingly, for the crystal field

environment of $CeRh_2As_2$ it has been reported that the Kondo temperature ≈30 K is comparable to the separation of the lowest energy cerium doublets [35]. As we discuss, a strong magnetic field will both have a tendency to spin polarize the cerium states, affecting the Kondo hybridization and potentially alter the relative contribution of the different $4f$ cerium states to the Fermi surface. Specifically the separation ($\Delta = 30$ K) of the $4f$ doublets is comparable to the applied field ($k_B\Delta = g\mu_B \approx 39$ T).

The low transition temperature ($T_0 = 0.5$ K) of the zero-field magnetic phase is consistent with f electrons that are only weakly hybridized. $CeRh_2As_2$ is a Kondo lattice system with the $4f$ electrons sitting on the f-multiplet at high temperatures and partially delocalized at low temperatures. In a magnetic field, the Kondo effect is gradually suppressed and the degree of $4f$ delocalization smoothly diminishes as the field increases; similarly, increasing temperature suppresses coherence and hence f-electron hybridization. A magnetic field applied parallel to the c axis may compete with Kondo hybridization, decreasing the contribution of the f electrons to the conduction bands at the Fermi energy, and, consequently, the scattering of other carriers. The system overall will then look like a better metal [see Fig. S2(d) [33]].

Because this transition corresponds to a significant increase in hole density, associated with a substantial fall in the chemical potential, it is also very plausible that this phase boundary is attributable to some form of field-induced valence transition, perhaps similar to that observed in $CeOs_4Sb_{12}$ [36]; valence transitions are also known to occur in several other heavy-fermion materials (e.g., $YbInCu_4$, URu_2Si_2, elemental Ce, Pu [36–40]), resulting in a variety of phenomena. In the current context, such a valence transition may represent the field driving $CeRh_2As_2$ from a phase with a higher Kondo temperature (and therefore spd and f hybridization, resulting in itinerant f-electron quasiparticles) to one with a lower Kondo temperature in which the f electrons are in effect localized on the $4f$ multiplet [37,39]. The latter removal of f electrons from the Fermi sea causes a fall in the chemical potential, resulting in an increase in the hole density, as is observed both in the present work and in $CeOs_4Sb_{12}$ [36]. In contrast to valence transitions in pure Ce and its alloys [39], the initial slope of the (H, T) phase boundary in Fig. 2(c) is positive. An analogous effect occurs in $CeOs_4Sb_{12}$ [36], attributed to proximity to a quantum-critical point associated with field-induced destruction of an AFM spin-density-wave (SDW) present below 1 K. The situation in $CeRh_2As_2$ may be closely related; the properties of its low-field, low-temperature (< 0.5 K) AFM state seen in μSR and NMR experiments are consistent with a SDW [25,27].

Another possible contribution to (or explanation for) the positive slope of the phase boundary in Fig. 2(c) may come from predictions of field induced quadrupolar ordering caused by coupling between the cerium Γ_7 ground state doublet and Γ_6; it results in an effectively localized quartet at high fields [35]. The latter effect may enhance the tendencies of the $4f$ electrons to quasilocalization, or even be functionally equivalent to a valence transition in removing the f electrons from the ensemble of itinerant carriers; the predicted phase boundary is qualitatively similar to Fig. 2(c).

To further elucidate the nature of this transition, we performed magnetization measurements (Fig. 3). For a field

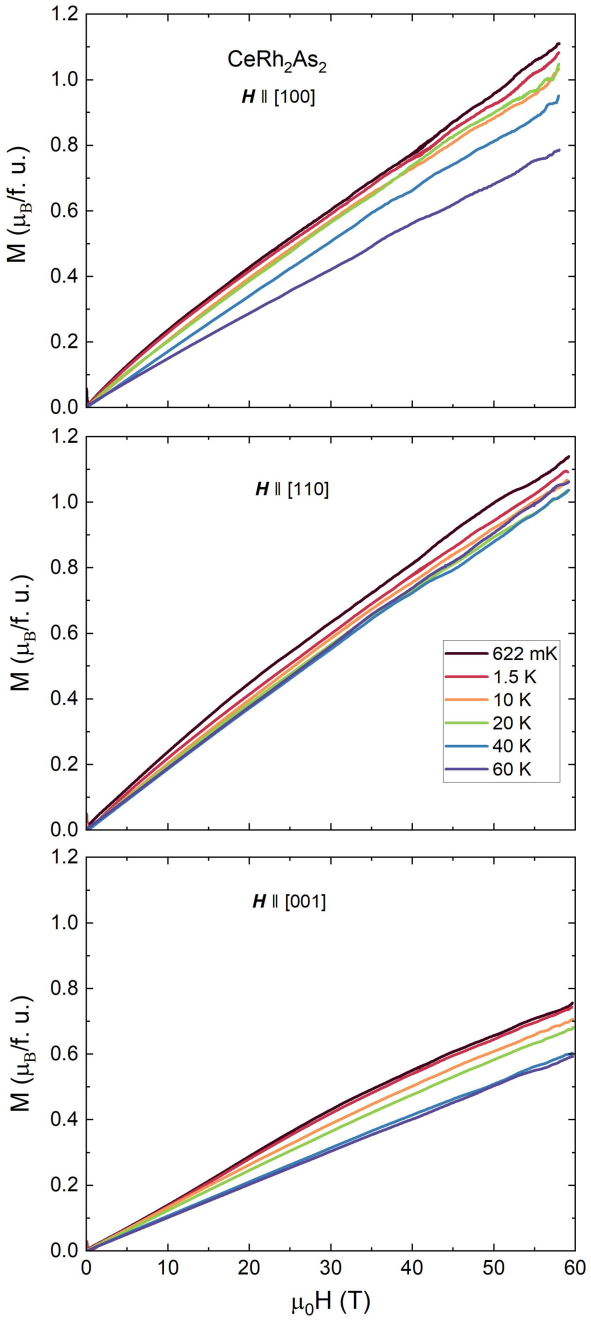


FIG. 3. Magnetization of $CeRh_2As_2$ measured up to 60 T with magnetic field along the [100], [110], and [001] crystallographic directions.

along the primary crystallographic axes ($\mathbf{H}\|[001]$, [100], [110]), the magnetization is largely featureless, suggesting an absence of metamagnetic transitions and no significant changes in net magnetic moment. The magnetization with $\mathbf{H}\|[001]$ shows a gentle inflection at about 24 T, which is consistent with valence transitions in Ce alloys and compounds; these affect the conductivity quite strongly (albeit over a relatively broad field range [36], as also seen in the present work) but lead to relatively weak changes in the magnetization [36,39]. The magnetization is smaller when $\mathbf{H}\|[001]$ than with field applied in-plane, indicating that c is the hard axis up to 60 T. When the field is applied in the in-plane directions, the magnetization as a function of field looks almost identical at 0.62 K, but it decreases with temperature faster when $\mathbf{H}\|[100]$ than with $\mathbf{H}\|[110]$. The lack of low-field in-plane anisotropy is consistent with the P4/nmm structure, with strong fields inducing a weak fourfold magnetic anisotropy.

III. CASCADE OF IN-PLANE FIELD INDUCED DENSITY WAVES

To further explore this in-plane anisotropy, structures were fabricated to enable control of both the in-plane field and current directions. Figure S3(a) (inset) [33] shows a 20 μm thick device patterned into a V-shape to enable simultaneous measurement of the resistance along the [100] and [110] directions. The magnetoresistance as a function of the field applied parallel to the current at various temperatures is plotted in Figs. S3(b) and S3(c) [33], showing multiple features and a strong in-plane anisotropy of the conductivity. Devices with a longer meandering current path were also prepared to increase the resistance while maintaining control of the predominant current direction (both parallel to [100] and [110]) to enable higher-fidelity measurement of these subtle changes in conductivity in pulsed fields; these devices are in Figs. 4(a) and 4(b). The resistance as a function of the field for a range of temperatures with $\mathbf{H}\|I$ is shown in Figs. 4(c) and 4(d). The overall behavior of $R(H)$ is similar to that observed in the V-shaped device, but the geometry enhances the resistance by an order of magnitude, indicating robustness of the observed in-plane field dependence (i.e., little or no sample to sample variation).

With $\mathbf{H}\|I\|[100]$, at 0.5 K, $R(H)$ decreases with increasing field, showing a minimum around 8 T, followed by an increase, with a broad maximum around 15 T. At higher fields $R(H)$ increases, exhibiting a maximum around 40 T before dropping quasilinearly to 60 T without any sign of saturation. With the field and current applied along [110] at 0.5 K, the resistance similarly decreases with increasing field, with a local maximum around 8 T, but is followed by almost constant $R(H)$ from 10 to 28 T. Around 30 T, there is a relatively sharp increase in $R(H)$ with a very broad maximum up to 40 T, whence $R(H)$ decreases linearly to 60 T. As temperature increases, all features move to higher fields.

To assess whether the changes in magnetoresistivity are sensitive to both the applied magnetic field and current direction, measurements were repeated with the field perpendicular to current, $\mathbf{H}\perp I$, i.e., $I\|[100]$ and $\mathbf{H}\|[010]$ [Fig. 4(e)], and $I\|[110]$ and $\mathbf{H}\|[1\bar{1}0]$ [Fig. 4(f)]. In the first case, $R(H)$ drops with increasing field, showing a change in slope around 8 T followed by a broad minimum above 20 T. After that, $R(H)$ increases, with a change in slope around 40 T. In Fig. 4(f), $R(H)$ shows a maximum around 8 T, followed by almost constant $R(H)$ from 10 to 30 T. At the latter field, a drastic increase in resistance is observed, followed by a very sharp decrease at 40 T and negative magnetoresistance to 60 T. Note also that significant hysteresis is observed between 30 and 40 T (Fig. S4 [33]), suggesting a first-order phase transition. For a selection of temperatures, these measurements were extended up to 73 T (Fig. S5 [33]) revealing an additional feature that moves to higher field on lowering T. Following the methodology employed for the c-axis MR, phase boundaries are ascribed to local minima/maxima in $\mathrm{d}R/\mathrm{d}H$ (Figs. S6, S7, S8 [33]).

For each field direction ([100], [110]), despite the form and magnitude of the magnetoresistance depending upon the orientation of the current (parallel or perpendicular to field), within the experimental error the phase boundaries appear solely determined by the magnetic field orientation. The T-H field phase diagrams with a typical resistance curve are presented in Fig. 5. Though not identical, the phase diagrams for $\mathbf{H}\|[010]$ and [110] are similar. Below 4 K, three closed field induced phases are observed, which evolve differently with increasing temperature.

Despite not being able to measure the Hall effect for in-plane-field orientations the changes in MR associated with the phase boundaries are not consistent with the large change in carrier density associated with the valence transition seen with the field parallel to [001]. Furthermore, given the "closed dome" nature of each phase in the T-H plane (solely determined by field orientation), the lack of observed change in magnetic susceptibility upon traversing the phases, and the field-induced anisotropy of the magnetoresistance in the in-plane phases are most consistent with a hierarchy of field-induced electronic density waves [41]. Figure S9 shows the temperature dependence of the resistance at different magnetic fields. Above 40 T there is a minimum, and the resistance increases slightly with decreasing temperature. However, the change is certainly much less dramatic than an onset of the activated temperature dependence expected for a semiconducting phase. Moreover, the temperature dependence changes with the current and magnetic field configurations, a behavior that is consistent with a field-induced density wave.

The calculated Fermi surface of $CeRh_2As_2$ [42–45] comprises multiple quasi-two and three-dimensional pockets that are strongly dependent upon the strength of hybridization and f-electron valence. However, a common

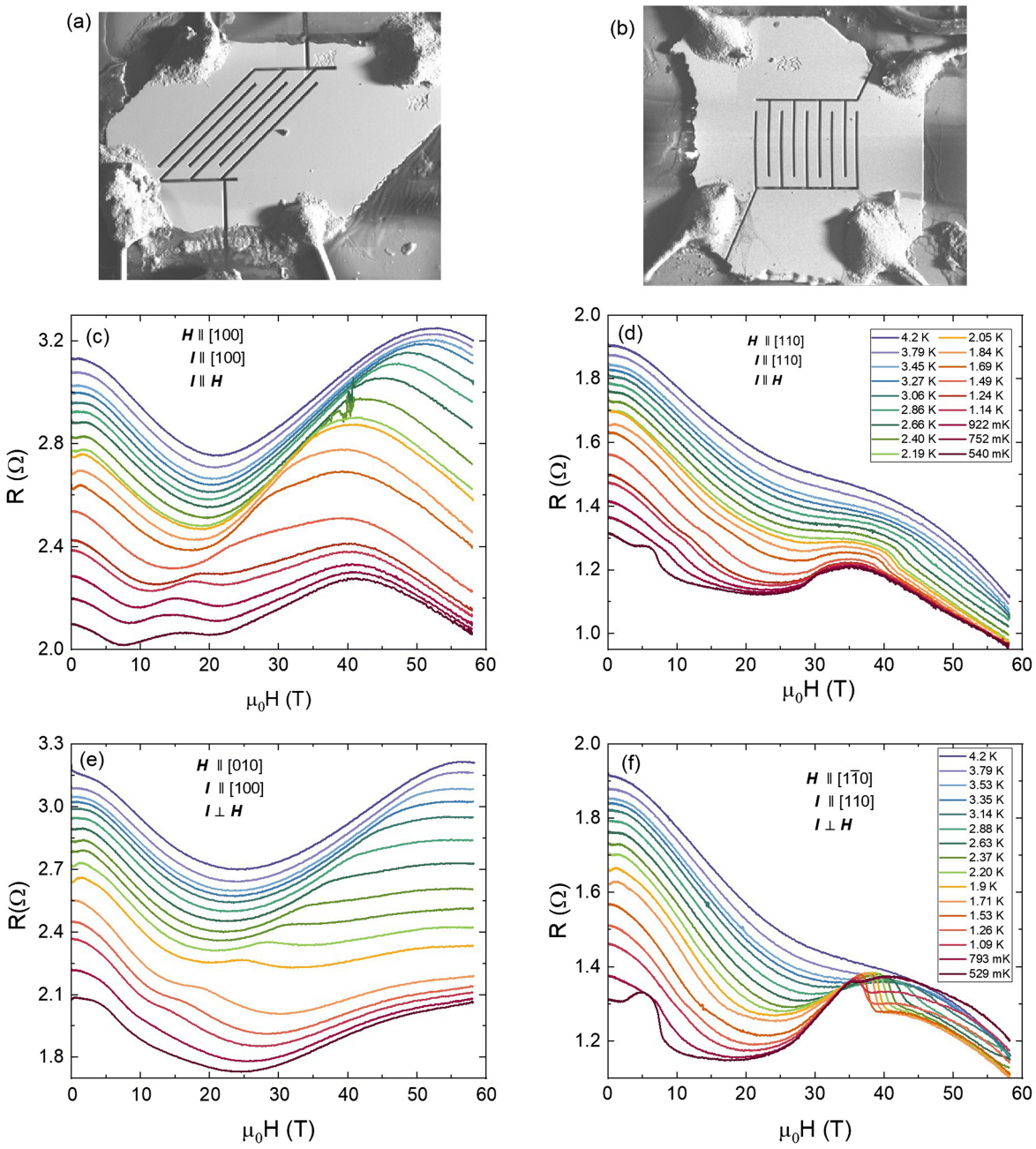


FIG. 4. Electron micrograph of the focused ion beam devices with springlike meanders microstructured along [100] (a) and [110] (b). Resistance versus magnetic field with $\mathbf{H}\|\mathbf{I}\|[100]$ (c), $\mathbf{H}\|\mathbf{I}\|[110]$ (d), $\mathbf{I}\|[100]$ and $\mathbf{H}\|[010]$ (e), $\mathbf{I}\|[110]$, and $\mathbf{H}\|[1\bar{1}0]$ (f).

feature appears to be the propensity for planar sections of the Fermi surface parallel to both [100] and [110] to appear at different heights (k_c) within the Brillouin zone. This suggests that field tuning of a density-wave nesting vector along [100] and [110] crystallographic directions is a likely explanation for the variation between in-plane phase boundaries. Density waves are both stabilized by magnetic fields owing to the effective reduction of dimensionality due to field-induced quasiparticle motion and ultimately destabilized by Zeeman splitting, in an analogous fashion to the Pauli paramagnetic limit of superconductors [46–48]. Comparing the maximum transition temperature (≈3.8 K) to the field that ultimately suppresses order (70 T) suggests that these density wave states are in the strong coupling limit [41]. Adding low-field heat-capacity data from Ref. [22] to the phase diagram for $\mathbf{H}\|[100]$ allows us to suggest that the T_0 transition observed previously with $\boldsymbol{H}\|[100]$ is most likely a continuation of the I_{100} phase boundary observed in the high field data. The phase below T_0 has previously been identified to as having both an antiferromagnetic and quadrupolar character [22–27]. The latter originates from the mixing of the ground state and

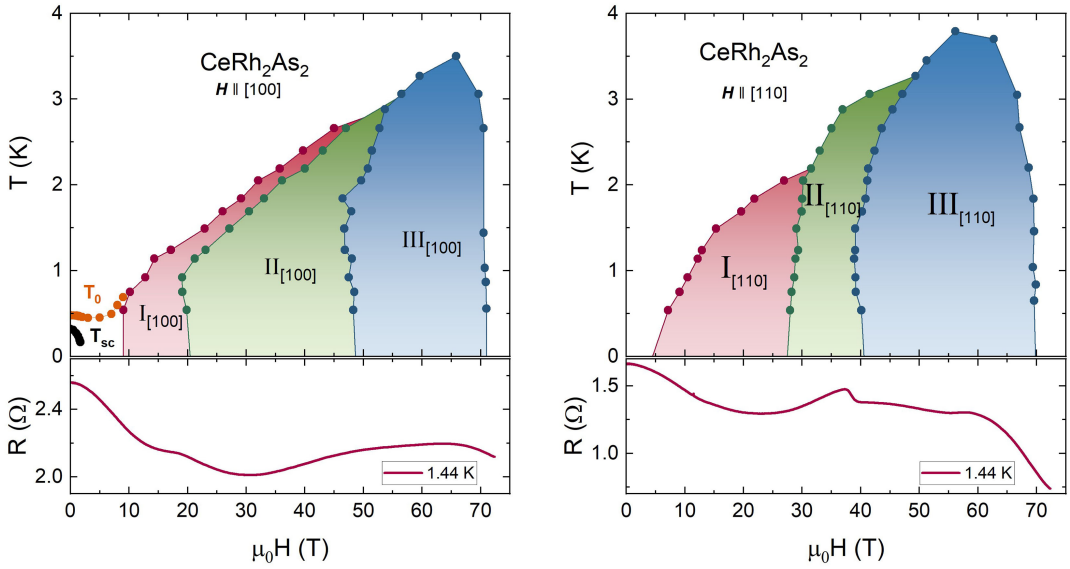


FIG. 5. Temperature: Magnetic field phase diagrams for $\mathbf{H}\|[100]$ and $\mathbf{H}\|[110]$ with representative resistance versus magnetic field curve measured at 1.44 K up to 73 T.

first excited state $4f$ doublets by the Kondo interaction and additionally by an in-plane magnetic field. The 30 K separation of the ground and first excited states combined with estimates of the Ce g factor [10] provide a natural explanation for the maximum transition temperature of the (in-plane) field-induced phases occurring at around 60 T where the two doublets are most mixed.

Although these transitions appear to be predominantly electronic in nature, given that $CeRh_2As_2$ is on the cusp of f-electron localization, it is interesting to speculate as to whether the observed phases involve purely charge, spin, or higher order density waves coupling multiple electronic degrees of freedom. According to Zanchi *et al.* [46], in quasi-1D systems with CDWs, the nesting vector does not get destroyed by applied magnetic field; instead unconventional DWs may be induced due to both charge- and spin-density-wave correlations [46]. $CeRhIn_5$ is not a 1D material; however, similar phenomena are proposed within a complex Fermi surface where both quasi-1D or 2D Fermi sheets coexist with 3D sheets [8]. The features observed in $CeRh_2As_2$ are remarkably similar to the cascade of field-induced charge density waves in $(Per)_2Pt(mnt)_2$ [47–49], graphite [50–52], and $CeRhIn_5$ [8]. When this is considered alongside the effect of magnetic field upon its superconducting phases, it becomes clear that $CeRh_2As_2$ is an important single material system for experimentally and theoretically investigating competition between electron-electron pairing, resulting in different symmetry superconducting states, and electron-hole pairing, resulting in density waves.

In this work, we present the first high field T-H phase diagram of $CeRh_2As_2$, and reveal the competition between correlated ground states and the role of magnetic field. Interestingly, there are phases of a different nature depending on the orientation of applied magnetic field. For $\mathbf{H}\|[001]$, there is a clear field-induced change of carrier density, perhaps attributable to a valence transition, whilst in-plane magnetic fields ($\mathbf{H}\|[100]$ and [110]) induce a cascade of density waves. This suggests that magnetic field not only tunes the pairing resulting in different symmetry superconducting ground states but also promotes density-wave ground states. As proposed in Ref. [22], many of the low-field properties of $CeRh_2As_2$ seem to be analogous to those of $CeRhIn_5$; our high-field studies further support those findings. Both valence transitions and density waves induced by magnetic field have been observed within other heavy fermion unconventional superconductors and metals, perhaps suggesting overarching physics common to these systems.

IV. METHODS

A. Single crystal synthesis and sample quality

Single crystals of $CeRh_2As_2$ were grown using the horizontal flux-growth technique. The detailed procedure is described in Ref. [30]. Crystal orientation was checked using a PROTO COS Laue diffraction camera. Low-field resistivity measurements were performed using a quantum design physical property measurement system (PPMS) equipped with a ^{3}He-^{4}He dilution refrigerator. These data were used to create the low-field–low-temperature phase diagram presented in Fig. 1(b). Points were selected using values from temperature sweeps at different constant magnetic fields at 90% and 50% of the resistance drop, and where the resistance reaches the zero value (see Fig. S1 [33]). The obtained phase diagram looks identical to that reported before, constructed using transport, heat capacity, magnetization, and magnetostriction

measurements [10,17,23,24,30]. These low-temperature and low-field data were essential to confirm the properties of the FIB-fabricated sample in the range where the phase diagram is already well known and established by various thermodynamic probes; hence the samples can be studied with confidence in high magnetic fields, where the physical properties remained unknown until this work.

B. Pulsed field magnetization measurements

The high field measurements were performed at the National High Magnetic Field Laboratory Pulsed-Field Facility at Los Alamos. The magnetization was measured using a compensated coil extraction magnetometer [53]. The crystal was placed in a 1 mm diameter ampoule which then can be moved in and out of the coil. The signal induced in the coil is proportional to the rate of change of magnetization with time $\mathrm{d}M/\mathrm{d}t$; the magnetization data are obtained by subtracting the integrated data without the sample present from that with the sample in the coil.

C. FIB devices fabrication and high field magnetotransport measurements

The resistivity and Hall effect data were measured on a microstructured device fabricated using a FIB FEI Helios Nanolab 600. The single crystal of $CeRh_2As_2$ was hand polished to 8–20 μm thickness. Transport and Hall measurements are extremely challenging in pulsed fields. Thinning down the sample and FIB fabrication made the experiment possible; however, the signal to noise is significantly lower in the Hall signal than that observed in the $R(H)$ curves. The noise values approach 10 $\mathrm{nV}/\sqrt{\mathrm{Hz}}$, close to the limit for room temperature amplification at frequencies of 100s of kHz. Parts of the sample were sputter coated with gold for electrical contacts, which were made using 25 μm Au wire and silver epoxy. At the final stage, the samples were microfabricated using FIB. In order to minimize the noise during the pulsed field measurements, each Au wire was attached to 50-gauge insulated copper wire twisted in current (I), voltage (V_{xx}) and Hall voltage (V_{xy}) pairs. For all measurement configurations a range of currents was applied without the observation of a nonlinear IV response; this was checked in both the directly digitized sample voltage sine wave and the harmonic content of the digital lock-in output, indicating that all reported data were measured in the Ohmic response regime.

ACKNOWLEDGMENTS

We would like to thank Philip Moll and Filip Ronning for constructive and helpful discussion. The work was performed at the National High Magnetic Field Laboratory, which is supported by National Science Foundation Cooperative Agreement No. DMR-2128556 and the State of Florida. J. B. and R. M. acknowledge support from Center for the Advancement of Topological Semimetals, an Energy Frontier Research Center funded by the U.S. Department of Energy, Office of Science through the Ames National Laboratory under Contract No. DEAC02-07CH11358 for the development of experimental capabilities including FIB sample preparation to enable the pulsed field measurements. J. S. acknowledges the DOE BES FWP "Science of 100 T" that permitted the development of experimental techniques used in this paper, and which supports measurements above 65 T.

DATA AVAILABILITY

The data that support the findings of this article are openly available [54].

[1] A. C. Hewson, *The Kondo Problem to Heavy Fermions* (Cambridge University Press, Cambridge, England, 1997).
[2] N. Maksimovic *et al.*, *Evidence for a delocalization quantum phase transition without symmetry breaking in* $CeCoIn_5$, Science **375**, 76 (2022).
[3] H. Hegger, C. Petrovic, E. G. Moshopoulou, M. F. Hundley, J. L. Sarrao, Z. Fisk, and J. D. Thompson, *Pressure-induced superconductivity in quasi-2D* $CeRhIn_5$, Phys. Rev. Lett. **84**, 4986 (2000).
[4] P. Gegenwart, Q. Si, and F. Steglich, *Quantum criticality in heavy-fermion metals*, Nat. Phys. **4**, 186 (2008).
[5] D. Aoki, W. Knafo, and I. Sheikin, *Heavy fermions in a high magnetic field*, C.R. Phys. **14**, 53 (2013).
[6] F. Ronning *et al.*, *Electronic in-plane symmetry breaking at field-tuned quantum criticality in* $CeRhIn_5$, Nature (London) **548**, 313 (2017).
[7] T. Helm *et al.*, *Non-monotonic pressure dependence of high-field nematicity and magnetism in* $CeRhIn_5$, Nat. Commun. **11**, 3482 (2020).
[8] P. J. W. Moll, B. Zeng, L. Balicas, S. Galeski, F. F. Balakirev, E. D. Bauer, and F. Ronning, *Field-induced density wave in the heavy-fermion compound* $CeRhIn_5$, Nat. Commun. **6**, 6663 (2015).
[9] S. Ran *et al.*, *Extreme magnetic field-boosted superconductivity*, Nat. Phys. **15**, 1250 (2019).
[10] S. Khim *et al.*, *Field-induced transition within the superconducting state of* $CeRh_2As_2$, Science **373**, 1012 (2021).
[11] G. Bruls, D. Weber, B. Wolf, P. Thalmeier, B. Lüthi, A. de Visser, and A. Menovsky, *Strain–order-parameter coupling and phase diagrams in superconducting* UPt_3, Phys. Rev. Lett. **65**, 2294 (1990).
[12] R. A. Fisher, S. Kim, B. F. Woodfield, N. E. Phillips, L. Taillefer, K. Hasselbach, J. Flouquet, A. L. Giorgi, and J. L. Smith, *Specific heat of* UPt_3*: Evidence for unconventional superconductivity*, in *Ten Years of Superconductivity: 1980–1990*, edited by H. R. Ott (Springer Netherlands, Dordrecht, 1993), pp. 189–192.
[13] T. Yoshida, M. Sigrist, and Y. Yanase, *Pair-density wave states through spin-orbit coupling in multilayer superconductors*, Phys. Rev. B **86**, 134514 (2012).
[14] K. Nogaki, A. Daido, J. Ishizuka, and Y. Yanase, *Topological crystalline superconductivity in locally noncentrosymmetric* $CeRh_2As_2$, Phys. Rev. Res. **3**, L032071 (2021).

[15] T. Hazra and P. Coleman, *Triplet pairing mechanisms from Hund's-Kondo models: Applications to* UTe_2 *and* $CeRh_2As_2$, Phys. Rev. Lett. **130**, 136002 (2023).
[16] A. Pourret and G. Knebel, *Driving multiphase superconductivity*, Science **373**, 962 (2021).
[17] J. F. Landaeta *et al.*, *Field-angle dependence reveals odd-parity superconductivity in* $CeRh_2As_2$, Phys. Rev. X **12**, 031001 (2022).
[18] X. Chen *et al.*, *Coexistence of near-E_F flat band and van Hove singularity in a two-phase superconductor*, Phys. Rev. X **14**, 021048 (2024).
[19] J. Ishizuka, K. Nogaki, M. Sigrist, and Y. Yanase, *Correlation-induced Fermi surface evolution and topological crystalline superconductivity in* $CeRh_2As_2$, Phys. Rev. B **110**, L140505 (2024).
[20] M. Sato and Y. Ando, *Topological superconductors: A review*, Rep. Prog. Phys. **80**, 076501 (2017).
[21] C. W. J. Beenakker, *Search for Majorana fermions in superconductors*, Annu. Rev. Condens. Matter Phys. **4**, 113 (2013).
[22] G. Chajewski and D. Kaczorowski, *Discovery of magnetic phase transitions in heavy-fermion superconductor* $CeRh_2As_2$, Phys. Rev. Lett. **132**, 076504 (2024).
[23] S. Mishra, Y. Liu, E. D. Bauer, F. Ronning, and S. M. Thomas, *Anisotropic magnetotransport properties of the heavy-fermion superconductor* $CeRh_2As_2$, Phys. Rev. B **106**, L140502 (2022).
[24] D. Hafner *et al.*, *Possible quadrupole density wave in the superconducting Kondo lattice* $CeRh_2As_2$, Phys. Rev. X **12**, 011023 (2022).
[25] S. Khim *et al.*, *Coexistence of local magnetism and superconductivity in the heavy-fermion* $CeRh_2As_2$ *revealed by* μSR *studies*, Phys. Rev. B **111**, 115134 (2025).
[26] K. Machida, *Violation of Pauli-Clogston limit in the heavy-fermion superconductor* $CeRh_2As_2$*: Duality of itinerant and localized 4f electrons*, Phys. Rev. B **106**, 184509 (2022).
[27] M. Kibune *et al.*, *Observation of antiferromagnetic order as odd-parity multipoles inside the superconducting phase in* $CeRh_2As_2$, Phys. Rev. Lett. **128**, 057002 (2022).
[28] P. J. W. Moll, *Focused ion beam microstructuring of quantum matter*, Annu. Rev. Condens. Matter Phys. **9**, 147 (2018).
[29] K. Semeniuk, M. Pfeiffer, J. F. Landaeta, M. Nicklas, C. Geibel, M. Brando, S. Khim, and E. Hassinger, *Exposing the odd-parity superconductivity in* $CeRh_2As_2$ *with hydrostatic pressure*, Phys. Rev. B **110**, L100504 (2024).
[30] G. Chajewski, D. Szymański, M. Daszkiewicz, and D. Kaczorowski, *Horizontal flux growth as an efficient preparation method of* $CeRh_2As_2$ *single crystals*, Mater. Horiz. **11**, 855 (2024).
[31] S. Onishi, U. Stockert, S. Khim, J. Banda, M. Brando, and E. Hassinger, *Low-temperature thermal conductivity of the two-phase superconductor* $CeRh_2As_2$, Front. Electron. Mater. **2** (2022).
[32] K. Semeniuk, D. Hafner, P. Khanenko, T. Lühmann, J. Banda, J. F. Landaeta, C. Geibel, S. Khim, E. Hassinger, and M. Brando, *Decoupling multiphase superconductivity from normal state ordering in* $CeRh_2As_2$, Phys. Rev. B **107**, L220504 (2023).
[33] See Supplemental Material at http://link.aps.org/supplemental/10.1103/m44c-tzrj for additional measurements and calculated derivatives used to determine phase boundaries.
[34] M. Scheffler, M. Dressel, M. Jourdan, and H Adrian, *Extremely slow Drude relaxation of correlated electrons*, Nature (London) **438**, 1135 (2005).
[35] P. Thalmeier, A. Akbari, and B. Schmidt, *Thermodynamics, elastic anomalies and excitations in the field induced phases of* $CeRh_2As_2$, New J. Phys. **27**, 033026 (2025).
[36] K. Götze *et al.*, *Unusual phase boundary of the magnetic-field-tuned valence transition in* $CeOs_4Sb_{12}$, Phys. Rev. B **101**, 075102 (2020).
[37] M. O. Dzero, *Crystal-field effects in the first-order valence transition in* $YbInCu_4$ *induced by an external magnetic field*, J. Phys. Condens. Matter **14**, 631 (2002).
[38] N. Harrison and M. Jaime, *Hidden valence transition in* URu_2Si_2*?*, arXiv:1902.06588.
[39] F. Drymiotis, J. Singleton, N. Harrison, J. C. Lashley, A. Bangura, C. H. Mielke, L. Balicas, Z. Fisk, A. Migliori, and J. L. Smith, *Suppression of the* $\gamma-\alpha$ *structural phase transition in* $Ce_{0.8}La_{0.1}Th_{0.1}$ *by large magnetic fields*, J. Phys. Condens. Matter **17**, L77 (2005).
[40] N. Harrison, J. B. Betts, M. R. Wartenbe, F. F. Balakirev, S. Richmond, M. Jaime, and P. H. Tobash, *Phase stabilization by electronic entropy in plutonium*, Nat. Commun. **10**, 3159 (2019).
[41] G. Gruner, *Density Waves In Solids* (CRC Press, Boca Raton, 2018).
[42] B. Chen *et al.*, *Exploring possible Fermi surface nesting and the nature of heavy quasiparticles in the spin-triplet superconductor candidate* $CeRh_2As_2$, Phys. Rev. B **110**, L041120 (2024).
[43] T. Chen *et al.*, *Quasi-two-dimensional antiferromagnetic spin fluctuations in the spin-triplet superconductor candidate* $CeRh_2As_2$, arXiv:2406.03566.
[44] Y. Wu *et al.*, *Fermi surface nesting with heavy quasiparticles in the locally noncentrosymmetric superconductor* $CeRh_2As_2$, Chin. Phys. Lett. **41**, 097403 (2024).
[45] A. Ptok, K. J. Kapcia, P. T. Jochym, J. Łażewski, A. M. Oleś, and P. Piekarz, *Electronic and dynamical properties of* $CeRh_2As_2$*: Role of* Rh_2As_2 *layers and expected orbital order*, Phys. Rev. B **104**, L041109 (2021).
[46] D. Zanchi, A. Bjeliš, and G. Montambaux, *Phase diagram for charge-density waves in a magnetic field*, Phys. Rev. B **53**, 1240 (1996).
[47] D. Graf, E. S. Choi, J. S. Brooks, R. T. Henriques, M. Almeida, and M. Matos, *High magnetic field induced charge density wave state in a quasi-one-dimensional organic conductor*, Phys. Rev. Lett. **93**, 076406 (2004).
[48] N. Harrison, R. D. McDonald, and J. Singleton, *Orbitally quantized density-wave states perturbed from equilibrium*, in *The Physics of Organic Superconductors and Conductors*, edited by A. Lebed (Springer, Berlin, Heidelberg, 2008), pp. 551–568.
[49] J. Singleton, R. D. McDonald, and N. Harrison, *High-field magnetoresistive effects in reduced-dimensionality organic metals and superconductors*, in *The Physics of Organic*

Superconductors and Conductors, edited by A. Lebed (Springer, Berlin, Heidelberg, 2008), pp. 247–276.

[50] H. Yaguchi and J. Singleton, *Destruction of the field-induced density-wave state in graphite by large magnetic fields*, Phys. Rev. Lett. **81**, 5193 (1998).

[51] H. Yaguchi and J. Singleton, *A high-magnetic-field-induced density-wave state in graphite*, J. Phys. Condens. Matter **21**, 344207 (2009).

[52] Z. Zhu, P. Nie, B. Fauqué, B. Vignolle, C. Proust, R. D. McDonald, N. Harrison, and K. Behnia, *Graphite in 90 T: Evidence for strong-coupling excitonic pairing*, Phys. Rev. X **9**, 011058 (2019).

[53] P. A. Goddard *et al.*, *Experimentally determining the exchange parameters of quasi-two-dimensional Heisenberg magnets*, New J. Phys. **10**, 083025 (2008).

[54] J. Blawat, G. Chajewski, D. Gnida, J. Singleton, O. A. Valenzuela, D. Kaczorowski, and R. McDonald, *Data for the Article "Competing electronic ground states in the heavy-fermion superconductor* $CeRh_2As_2$*"*, 10.17605/OSF.IO/XKN4Z (2025).